frontiers | Frontiers in Oncology

TYPE Original Research
PUBLISHED 16 March 2023
DOI 10.3389/fonc.2023.1126094

Check for updates

OPEN ACCESS

EDITED BY
Luis Alexandre Muehlmann,
University of Brasilia, Brazil

REVIEWED BY
Suresh Thangudu,
Kaohsiung Chang Gung Memorial Hospital, Taiwan
Linawati Sutrisno,
Chongqing University, China
Yishen Zhu,
Nanjing Tech University, China

*CORRESPONDENCE
Hong Li
lihong0708@sina.com

†These authors have contributed equally to this work

SPECIALTY SECTION
This article was submitted to Skin Cancer, a section of the journal Frontiers in Oncology

RECEIVED 17 December 2022
ACCEPTED 23 January 2023
PUBLISHED 16 March 2023

CITATION
Zhang L, Liu X, Mao Y, Rong S, Chen Y, Qi Y, Cai Z and Li H (2023) Inhibition of melanoma using a nanoceria-based prolonged oxygen-generating phototherapy hydrogel.
Front. Oncol. 13:1126094.
doi: 10.3389/fonc.2023.1126094

COPYRIGHT
© 2023 Zhang, Liu, Mao, Rong, Chen, Qi, Cai and Li. This is an open-access article distributed under the terms of the Creative Commons Attribution License (CC BY). The use, distribution or reproduction in other forums is permitted, provided the original author(s) and the copyright owner(s) are credited and that the original publication in this journal is cited, in accordance with accepted academic practice. No use, distribution or reproduction is permitted which does not comply with these terms.

Inhibition of melanoma using a nanoceria-based prolonged oxygen-generating phototherapy hydrogel

Lidong Zhang[1†], Xiaoguang Liu[2†], Yinghua Mao[3], Shu Rong[3], Yonghong Chen[3], Yong Qi[4], Zhipeng Cai[3] and Hong Li[3*]

[1]Institute of Military Preventive Medicine, Army Medical University (Third Military Medical University), Chongqing, China, [2]Department of Gynecology, Women's Hospital of Nanjing Medical University (Nanjing Maternity and Child Health Care Hospital), Nanjing, China, [3]Centre for Diseases Prevention and Control of Eastern Theater, Nanjing, China, [4]Huadong Research Institute for Medicine and Biotechniques, Nanjing, China

Tumor hypoxic environment is an inevitable obstacle for photodynamic therapy (PDT) of melanoma. Herein, a multifunctional oxygen-generating hydrogel loaded with hyaluronic acid-chlorin e6 modified nanoceria and calcium peroxide (Gel-HCeC-CaO_2) was developed for the phototherapy of melanoma. The thermo-sensitive hydrogel could act as a sustained drug delivery system to accumulate photosensitizers (chlorin e6, Ce6) around the tumor, followed by cellular uptake mediated by nanocarrier and hyaluronic acid (HA) targeting. The moderate sustained oxygen generation in the hydrogel was produced by the reaction of calcium peroxide (CaO_2) with infiltrated H_2O in the presence of catalase mimetic nanoceria. The developed Gel-HCeC-CaO_2 could efficiently alleviate the hypoxia microenvironment of tumors as indicated by the expression of hypoxia-inducible factor -1α (HIF-1α), meeting the "once injection, repeat irradiation" strategy and enhanced PDT efficacy. The prolonged oxygen-generating phototherapy hydrogel system provided a new strategy for tumor hypoxia alleviation and PDT.

KEYWORDS

photodynamic therapy, hydrogel, melanoma, nanaoceria, hypoxia alleviation

1 Introduction

The global morbidity and mortality of melanoma are increased dramatically, which is still one of the severe threats to public health (1–3). However, traditional tumor treatment often confronts obstacles due to visible toxic side effects and drug resistance (4). Recently, synergetic photodynamic therapy (PDT) has been introduced to overcome melanoma and has shown great potential in the field of tumor therapy (5, 6). As a noninvasive technology, PDT addresses spectacular advantages such as high localized tissue damage and minimal side effects (7). In the PDT process, photosensitizers such as chlorin e6 (Ce6) accumulated in tumor tissues are usually activated and energized by a specified light, resulting in reactive oxygen species (ROS) generation and singlet oxygen ($^1O_2$) in the presence of biological substrates and oxygen (8). Therefore, oxygen and photosensitizer contents in tumor tissues are restrictive factors for PDT reaction and cytotoxicity (9). However, the therapeutic efficacy

of PDT is often unsatisfactory because of the hypoxic microenvironment in most malignant tumors and rapid drug metabolism-induced short-term effects (10–12). It is of great significance to alleviate hypoxia and prolong photosensitizer supply in the tumor environment for enhancing PDT efficacy.

Several efforts have been conducted to overcome tumor hypoxia, such as water splitting (13, 14), respiratory inhibitor (15, 16), O_2-evolving agents (17, 18), catalase (19, 20), and nanoscale metal-organic framework (21, 22). Among them, catalase could effectively improve the efficacy of oxygen supply and PDT treatment because of the catalytic decomposition of elevated H_2O_2 in the tumor environment (23, 24). However, the poor stability, cost, and limited catalyst capacity restrict the application of natural catalase. These limitations have emerged the nanoenzymes, which are defined as nanomaterials with enzyme-like characteristics (25, 26). Numbers of nanomaterials based on iron oxides (27), copper oxides (28, 29), vanadium oxides (30, 31), and noble metals (Au, Ag, Pt, Pd) (32–36) have been reported to mimic catalase activity.

Cerium nanoparticles (CeNPs) are a remarkably versatile rare earth nanomaterial with excellent catalytic activities (37, 38). It has been reported to mimic multiple types of enzymes due to the electron shuttle between their mixed oxidation states (Ce^{3+}/Ce^{4+}) and has emerged as a fascinating material in biological fields (39). Recently, we demonstrated that chemically cytotoxic and oxygen-carrying CeNPs could act as a nanocarrier to deliver photosensitizers into tumor cells, resulting in enhanced PDT efficacy (40, 41). In this study, to obtain sufficient oxygen generation for PDT, the CeNPs nanocarrier was introduced into the system and used as an ideal renewable catalase-like enzyme to catalyze the reaction of CaO_2 and H_2O. Herein, we designed a prolonged oxygen-generating phototherapy hydrogel system (Gel-HCeC-CaO_2) to improve the therapeutic efficacy of PDT in treating melanoma.

2 Materials and methods

2.1 Chemicals and reagents

Poloxamer P407 (F127) and Poloxamer P188 (F68) were purchased from BASF,Germany. H_2O_2 (technical grade, 30%) was offered by Aladdin,China. CaO_2, Cerium (III) nitrate hexahydrate, Docusate sodium(AOT), and Alendronate sodium were offered by Sigma Aldrich,USA. Chlorin e6 (Ce6) was offered by Frontier Scientific, Inc, USA. HA with a molecular weight (MW) of 17kDa was purchased from Lifecore Co. Dulbecco's modified Eagle's medium (DMEM), Fetal bovine serum (FBS) and Trypsin-EDTA (0.25%) were purchased from Gibco,USA. The Cell counting kit-8 (CCK-8 kit) were purchased from Dojindo,Japan. Trizol reagent was offered by Invitrogen,USA. PrimeScript RT Master Mix was purchased from Takara,Japan. SYBR Green PCR Master Mix was purchased from Applied Biosystems,USA. All chemicals and reagents were of analytical grade.

2.2 Synthesis of materials

The naked cerium oxide nanoparticles (MCeNPs), cerium oxide nanoparticles-alendronate (CeNPs-AL), hyaluronic acid-chlorin e6 modified nanoceria (HCeC), and Gel-HCeC-CaO_2 were prepared as described in the literature (17, 42).

MCeNPs: 0.4548 g AOT and 1.5 ml $Ce(NO_3)_3{\cdot}6H_2O$ aqueous solution(0.1 M) were added to 30 ml methylbenzene under potent stirring for 45 min (4500 rpm/min). Then H_2O_2 was added using a pipette tip slowly under potent stirring for 1 h (4500 rpm/min).

CeNPs-AL: 20 mg AL,200 mg Na_2CO_3, and 10 ml MCeNPs were added to 5 ml ddH_2O under potent stirring for 24 h, then centrifugal (5 min,3000 rpm). After that, we used a dialysis bag (Thermo, 10kDa) to dialyze the acquired CNPs-AL for 24 h.

HCeC: 0.5 mL $Ce(NO_3)_3{\cdot}6H_2O$ aqueous solution(0.1 M) were added to 10 mL HA aqueous solution(5 $mg{\cdot}ml^{-1}$) at 37 °C under potent stirring. After 15 min, 0.8 ml sodium hydroxide (NaOH) (1M) was added to the mixture and stirred for 30 min. Then, 400 µl Ce6 (10 mM) was quickly added and stirred for 5.5 h. After that, the dialysis bag (Thermo, 10 kDa) was used to dialyze the acquired HCeC for 24 h in dark and rinsed with water repeatedly in a sleeve tube (Millipore, 30 kD). The acquired HCeC were dispersed in ddH_2O (HCe not contained Ce6).

Gel-HCeC-CaO_2: 0.26 g Poloxamer407 (F127),7.5 mg CaO_2 were mixed in a 1 mL bottle, then 400 µL PoloxamerP188 (F68) and 313 µL HCeC were added to it. At last, ddH_2O was added to 1 mL and acquired Gel-HCeC-CaO_2 system (Gel not contained CaO_2 and HCeC, Gel-CaO_2 only included CaO_2).

2.3 Characterization of HCe and HCeC

The zeta potential of the HCe and HCeC were determined using dynamic light scattering(Invitrogen, America). The hydration of nanoparticles was determined by dynamic light scattering (DLS) analysis. The HCe and HCeC were characterized by HR-TEM (FEI, America) at an accelerating voltage of 200 kV. The fluorescence spectra of Ce6, HCe, and HCe6 were determined by Fluoromax-4 spectrofluorometer (Horiba Jobin Yvon Inc, France) at 405nm excitation light. The absorption spectra of Ce6, HCe, and HCeC solution were determined by a UV spectrophotometer (KAIAO, China). Moreover, the HCe and HCeC were cultured with ddH_2O、PBS 、DMEM、DMEM+ 10% FBS for 24 h to observe the stability. The photosensitivity of HCeC was detected by singlet oxygen sensor green reagent (SOSG). And we mixed the HCeC with 50 mM H_2O_2 to show the CAT-like activity of the HCeC.

2.4 Sol-Gel transition behavior of the Gel-HCeC-CaO_2 system

1 mL Gel and Gel-HCeC-CaO_2 solution were added into a 10 mL bottle, then put the bottle into a 37 °C water bath at a different time until the solution transformed to gel, recording the time (43). The test

Abbreviations: PDT, photodynamic therapy; Gel-HCeC-CaO2,oxygengenerating hydrogel loaded with hyaluronic acid-chlorin e6 modified nanoceria and calcium peroxide; Ce6, chlorin e6; HA, hyaluronic acid; CaO2, calcium peroxide; HIF-1a, hypoxiainducible factor -1a; ROS, reactive oxygen species; CeNPs, cerium nanoparticles; AOT, docusate sodium; NaOH, sodium hydroxide; DMEM, dulbecco's modified Eagle's medium; FBS, fetal bovine serum.

tube inverting method was used to determine the sol-gel transition behavior of the hydrogel (44), 1 mL Gel and Gel-HCeC-CaO_2 solution was placed in a 10 mL bottle at -20 °C, 4 °C, 25 °C, and 37 °C to observe the solution transformed to gel. 1 mL Gel-HCeC-CaO_2 solution was placed in a 10 mL bottle and incubated at 37 °C for 5 min to gel. 1 mL PBS (pH = 7.4, 37 °C) and $CaCl_2$ solution were gently added into the bottle as a release medium. The bottles were shaken at the speed of 50 rpm in a thermostatic shaker (HENGZI, China) at 37°C while the weight of the gel was measured every 20 min.

2.5 Oxygen generation of the Gel-HCeC-CaO_2 system

N_2 was injected into 30 mL PBS for 30 min to produce the deoxygenated PBS. The deoxygenated PBS was divided into two groups, and the PH was adjusted by concentrated hydrochloric acid to 5.4 and 7.2, respectively. 5 mL Gel-HCeC-CaO_2 solution were put into a 50 mL centrifuge tube and incubated at 37 °C for 5 min to gel. Then, 30 mL deoxygenated PBS (PH=7.2/5.4, 37 °C) was added into Gel-HCeC-CaO_2 solution. Afterward, we added 10 mL cooking oil isolate deoxygenated PBS and air. We used the Dissolved Oxygen Meters (Mettler, Switzerland) to detect oxygen generation.

2.6 Cell experiment and design

We obtained the murine melanoma cells (B16F10) lines from the Chinese Academy of Sciences cell bank. Cells were cultured in RPMI 1640 culture medium containing 10% FBS and 1% penicillin-streptomycin in a controlled environment (37 °C, 95% air, 5% CO_2).

Cell migration assay: B16F10 cells were seeded into 6-well plates and allowed to grow 80%-90% confluence. We used a sterile 20 μL pipette tip to scrape the confluent monolayer to form a cell-free zone. Then, B16F10 cells were incubated with HCeC (1 μg ·mL^{-1}) or Gel-HCeC-CaO_2 (1 μg ·mL^{-1}) for 24 h and irradiated by the 660 nm laser (200 mW/cm^2) irradiation for 5 min (45). Cells were photographed at 0, 24, and 48 h with a light microscope (Olympus, Japan).

Cytotoxicity assays: B16F10 cells were seeded at an initial density of 1 × 10^4 in 200 μl RPMI 1640 medium. After 24 h, cells were incubated with HCeC (0,0.125,1.25,12.5,25 μg·mL^{-1}, dark, laser) or Gel-HCeC-CaO_2 (0,0.005,0.05,0.5,1 μg·mL^{-1}, dark, Laser). The laser group received the 660 nm laser (200 mW/cm^2) irradiation for 5 min after incubation at 24 h. After 48 h, we added 10 μL CCK-8 solution to each well and detected the absorbance at 450 nm.

2.7 Animal experiment and design

Animal model: All BALB/c-nu mice animal procedures were approved by SPF Biotechnology Co., Ltd in our experiments. The melanoma cancer model was generated by subcutaneous injection of B16F10 cell (5×10^5) suspended in PBS into the flank region of the right back of BALB/c mice and allowed them to grow into solid tumors.

Biodistribution of Gel-HCeC-CaO_2 in B16F10 tumor-bearing mice: Mice were injected with 100μL Ce6, HCeC, and Gel-HCeC-CaO_2 after the tumor volume reached about~65 mm^3. We used an *in vivo* imaging system (Perkin Elmer, America) to observe the mice at 0,4, and 20 h after injection. And the major organs such as the liver, spleen, kidney, heart, lung, and tumor were excised for further imaging analysis.

Antitumor on orthotopic B16F10 model: When the tumor size achieved ~65 mm^3, B16F10 tumor-bearing mice were randomly divided into eight groups (n=6/group): PBS (100μL,dark),Gel-CaO_2 (100μL,dark),HCeC (100μL,dark),HCeC (100μL,laser),HCeC (100μL,laser*2),Gel-HCeC-CaO_2 (100μL,dark),Gel-HCeC-CaO_2 (100μL,laser), and Gel-HCeC-CaO_2 (100μL,laser*2). The laser group was irradiated with 660 nm laser (200 mW/cm^2) irradiation for 5 min at 4 h or 20 h. And we recorded the body weights and tumor volumes of mice every 2 days (46). The tumor volumes were measured with a digital caliper and calculated as the following formula: $width^2\times length\times0.5$.

Histological analysis and anti-metastatic activity of mice: The tumors of all mice were collected and subjected to the H&E staining or TUNEL assays after the mice were sacrificed. We used a light microscope (Olympus, Japan) to observe the histological change. At the same time, the lungs of mice were also excised and photographed (47).

2.8 Quantitative polymerase chain reaction

The oligonucleotide primers were designed by Sangon Biotech (Shanghai, China) and listed in Table 1. The total RNA was extracted by TRIzol reagent and quantified by NanoDrop2000 spectrophotometer (Thermo Fisher Scientific, USA). The PrimeScript RT Master Mix and SYBR Green PCR Master Mix were used for performing the qPCR (48).

2.9 Statistical analysis

The data were expressed as mean values ± SEM, including at least three biological replicates. The Student's t-test and one-way analysis of variance (ANOVA) were utilized to determine the statistical significance of differences among groups. Statistical values are indicated according to the following scale: $_*p < 0.05$, $_{**}p < 0.01$, $_{***}p < 0.001$. All statistical analyses were performed by SPSS 19.0 software.

TABLE 1 Primer sequences of target genes for qPCR.

Gene	Species	Forward primer sequence (5'-3')	Reverse primer sequence (5'-3')
β-actin	mouse	CCACCATGTACCCAGGCATT	CGGACTCATCGTACTCCTGC
TNF-α	mouse	GAATGAAGTGCACCCTAACAAG	GAGGAATGGGTTCACAAATCAG

3 Results

3.1 Characterization of HCe and HCeC

The MCeNPs was synthesized by the microemulsion method (49). As shown in Supplementary Figure 1, the solution was milky white in the process of magnetic stirrers, which stratified overnight. The upper popcorn liquid was a toluene organic phase containing MCeNPs and the underlying dark yellow liquid was an aqueous phase containing CeNPS-Al. Due to the lack of effective surface protection, MCNPs was agglomerated in solution and cleared by the endothelial reticular system (ERS) in the body. Therefore, HCe and HCeC were synthesized by probing the interaction between CeNPs and HA to improve the stability of MCeNPs. To measure the size distribution of HCe and HCeC, we performed the DLS. As shown in Figure 1A, the average diameter of HCeC was approximately 25.60 nm while HCe was about 19.86 nm, because the Ce6 molecule increased the molecular diameter of HCe. And the zeta potential of the HCeC was approximately -6mV and the HCe was -5.6mV in Figure 1B, owing to the presence of the carboxyl group in Ce6. To examine the structure of the HCe and HCeC, the detailed morphology was characterized by HR-TEM. Due to the protective effect of HA (50), we found the size of HCe and HCeC are about 2-3nm and 3-4nm, showing good dispersion in water in Figure 1C. The Ce^{3+}/Ce^{4+} ratio is crucial for the enzyme-mimetic activity, the X-ray photoelectron spectroscopy (XPS) analysis of HCe and HCeC showed high Ce^{3+}/Ce^{4+} ratio in Figures 1D, E and Supplementary Figures 2A–C. Besides, the results of Fourier transform infrared spectra (FT-IR) showed that HA was conjugated to nanoceria successfully in Supplementary Figure 2D.

To verify that Ce6 was linked to HCe, the fluorescence spectra of Ce6, HCe, and HCeC were determined by a fluorescence spectrometer at 405 nm excitation light in Figure 1F, and the characteristic fluorescence peaks of Ce6 were between 640-690nm. Owing to the electron transfer between HCe and Ce6, HCeC showed significant fluorescence quenching compared with Ce6. The successful preparation of HCeC was validated by UV–vis absorption spectroscopy in Figure 1G. The characteristic absorption peak of Ce6 was at 404nm, with the Q wave between 500-700nm. The absorption peak of HCeC was similar to Ce6 besides a little red shift, which indicated that Ce6 had been successfully covalently linked to HCe. To explore the stability of nanomaterial, HCe and HCeC were mixed in a series of physiological solutions (water, PBS, DMEM, DMEM+10% FBS) for 24 h. As shown in Supplementary Figure 2E, we found there were no obvious agglomeration and precipitation of HCe and HCeC. These results indicated that HA modification could improve the stability of CeNPs effectively as literature report (51, 52). Besides, we found that the mass ratio of Ce to Ce6 of the HCeC is about 1:0.33 Supplementary Figures 2F, G and the HA modification could not affect the photosensitivity of HCeC in Figure 1H. The HCeC showed high CAT-like activity in Figures 1I, J. Therefore, we demonstrated that HA had been successfully modified on the surface of nano-sized cerium oxide and covalently bound to Ce6, which provided a foundation for further biological application.

3.2 Characterization of the Gel-HCeC-CaO_2 system

Hydrogel was a kind of polymer material that had been widely studied at present (53), which could be converted between liquid and solid state with a change of temperature. To show the sol-gel transition behavior of the hydrogel by the test tube inverting method

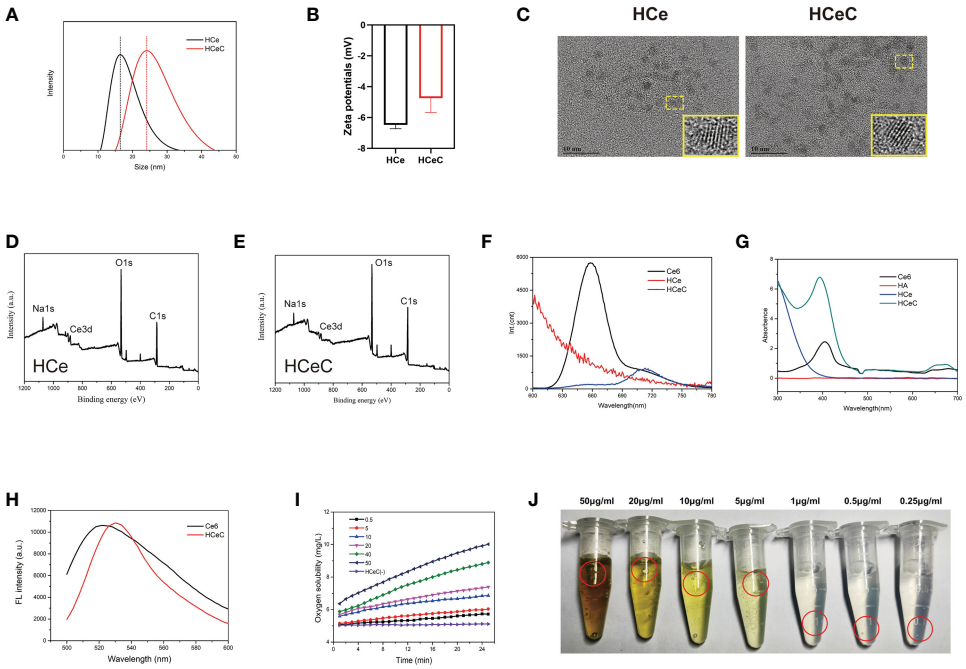

FIGURE 1
Characterization of HCe and HCeC. **(A)** DLS of HCe and HCeC. **(B)** Zeta potential of HCe and HCeC. **(C)** TEM of HCe and HCeC. **(D)** XPS analysis of HCe. **(E)** XPS analysis of HCeC. **(F)** Fluorescence spectra of Ce6, HCe, and HCeC. **(G)** UV–vis absorption spectroscopy of Ce6, HA, HCe and HCeC. **(H)** Photosensitivity of HCeC. **(I, J)** The CAT-like activity of HCeC.

(44), the Gel and Gel-HCeC-CaO_2 were liquid at -20°C、4°C 、25°Cand 37°C. As shown in Figure 2A, the liquid transformed into gel at -20°C and 37°C and the sol state at 4°C and 25°C. With the extension of the bath time at 37°C, the hydrosol transformed into the gel phase gradually, and the rheological temperature was affected by the addition of CaO_2 and HCeC. The gelation time of Gel-HCeC-CaO_2 was approximately 9 s with the Gel needing 12 s and more time in Figure 2B. To observe the corrosion behavior of the Gel, the release experiment *in vitro* was performed, which showed the gel is almost completely dissolved at approximately 6 h in Figure 2C, following zero-order kinetics. Besides, the UV–vis absorption spectroscopy was used to investigate the photophysical properties of HCeC, Gel, Gel-CaO_2, and Gel-HCeC-CaO_2 in Figure 2D, and the absorption peak of Gel-HCeC-CaO_2 was similar to HCeC, indicating that HCeC was mixed with the gel.

Furthermore, owing to the catalase activity of HCeC, the O_2 generation of Gel-HCeC-CaO_2 *in vitro* was detected. As shown in Figure 2E, the generation rate of oxygen from Gel-HCeC-CaO_2 (PH=7.2) was fast compared with other groups, indicating that the catalase activity of HCeC was influenced by the PH value. Owing to the catalase activity of the Gel-HCeC-CaO_2 being affected by PH (54), the catalase activity of the Gel-HCeC-CaO_2 was the highest under neutral conditions while reducing the catalase activity under acidic conditions. Therefore, the Gel-HCeC-CaO_2 could release oxygen slowly to relieve tumor hypoxia in the acidic tumor microenvironment.

3.3 *In vitro* PDT of HCeC and Gel-HCeC-CaO_2 system

To detect the phototoxicity of Gel-HCeC-CaO_2, cell viability was measured by CCK-8. There was almost no significant phototoxic effect observed in B16F10 cells treated with HCeC with or without irradiation in Figure 3A. However, the B16F10 cells treated with Gel-HCeC-CaO_2 (Laser) had a significant effect on B16F10 cells compared with Gel-HCeC-CaO_2 (Dark) in Figure 3B. Because the Gel-HCeC-CaO_2 (Laser) could release oxygen to improve the PDT efficiency, and produce a large number of $^1O_2$ and ROS to kill tumor cells. Moreover, the H_2O_2 (300 μM) could almost kill 50% of B16F10 cells owing to the toxicity in Supplementary Figure 3A, but the H_2O_2 (100 μM) had almost no effect, confirming that the toxicity of Gel-HCeC-CaO_2 was not caused by H_2O_2. To test the migration of B16F10 cells treated with Gel-HCeC-CaO_2 (Laser), we performed the scratch test. As shown in Figure 3C, the migration ability of B16F10 cells in the Gel-HCeC-CaO_2 (Laser) group was significantly lower compared with other groups. Therefore, the Gel-HCeC-CaO_2 (Laser) could enhance PDT efficiency and kill B16F10 cells significantly.

3.4 *In vivo* biodistribution of Gel-HCeC-CaO_2 system

To show the biodistribution of Gel-HCeC-CaO_2 *in vivo*, the fluorescence of Ce6, HCeC, and Gel-HCeC-CaO_2 in mice was detected at 0 h,4 h, and 20 h post-injection. As shown in Figure 3D, only a small amount of fluorescence appeared at the tumor site in Ce6 and HCeC group whereas predominantly observed in the Gel-HCeC-CaO_2 group at 20 h, suggesting that the good retention of the Gel-HCeC-CaO_2 in the mice. The biodistribution of the nanomaterials in mice was quantitatively analyzed in Figure 3E. Fluorescence imaging of some organs like lungs, liver, and kidneys showed that free Ce6 and HCeC were rapidly cleared over time up to 20 h, and the Gel-HCeC-CaO_2 had the good retention of the tumor to improve the PDT efficiency.

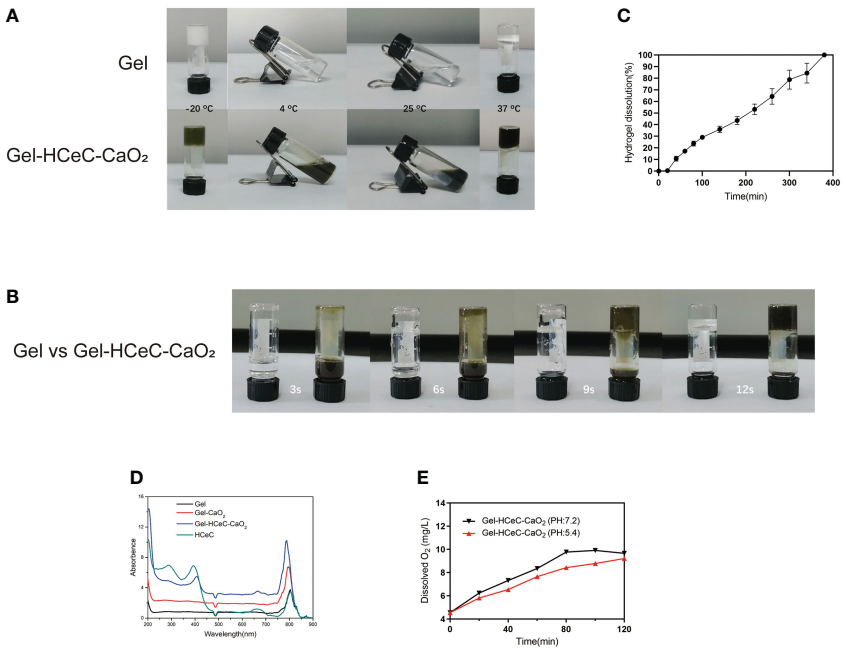

FIGURE 2
Characterization of the Gel-HCeC-CaO_2 system. **(A)** The sol-gel transition behavior of Gel and Gel-HCeC-CaO_2 system. **(B)** The gelation time of Gel and Gel-HCeC-CaO_2. **(C)** The corrosion behavior of the Gel-HCeC-CaO_2. **(D)** The photophysical properties of HCeC, Gel, Gel-CaO_2, and Gel-HCeC-CaO_2. **(E)** The O_2 generation of Gel-HCeC-CaO_2.

3.5 *In vivo* photodynamic effect of Gel-HCeC-CaO_2 system

The athymic nude mouse xenograft B16F10 model was generated for photodynamic therapy of melanoma. To examine the PDT efficiency of different materials to reduce tumor progression in the athymic nude mouse xenograft B16F10 model, 100μL PBS, Gel-CaO_2, HCeC, Gel-HCeC-CaO_2 were intravenously injected into the mice at 1 week after engraftment, and the NIR irradiation (660 nm, 200 mW/cm^2, 5 min) was administered to the tumor site at 4 h and 20 h post-injection in the laser groups in Supplementary Figures 3B, C. The tumors of mice in each group were photographed, the Gel-HCeC-CaO_2 group could significantly inhibit the B16F10 tumor progression in Figures 4A, B. As shown in Figures 4C, D, the HCeC and Gel-HCeC-CaO_2 groups showed significant tumor regression with a reduction of the tumor volume by ~42%, indicating the chemotherapy toxicity of the HCeC. The laser groups which irradiated one time could delay B16F10 tumor progression by~69%, indicating that HCeC had obvious phototherapy toxicity. The Gel-HCeC-CaO_2(Laser*2)had high tumor growth inhibition than HCeC(Laser*2), showing that Gel-HCeC-CaO_2 could satisfy repeat PDT therapy.

The tunnel assay confirmed that the Gel-HCeC-CaO_2 (Laser) group induce apoptosis of B16F10 cells *in vivo* in Figure 4E. Furthermore, hematoxylin and eosin (H&E) staining revealed large areas of necrosis, inflammatory cell infiltration and broken blood vessels of tumor tissue in Gel-HCeC-CaO_2 (Laser*2) group in Figure 4F. Hypoxia-inducible factor 1 α (HIF-1 α) was an important transcriptional regulator, which was crucial for tumor progression (55). The Gel-HCeC-CaO_2 system could significantly inhibit the expression of HIF-1 α compared with the HCeC in Figure 4G, indicating that Gel-HCeC-CaO_2 could alleviate the hypoxia of the tumor microenvironment. Besides, there were no metastatic tumor nodules observed in the lungs of the mice in Supplementary Figure 3D. To show the systemic toxicity of materials, we observed the body weight and histological change of mice. As shown in Figure 4H, the treatment could not change the body weight of mice. Therefore, the Gel-HCeC-CaO_2 (Laser) could reduce tumor progression in the athymic nude mouse xenograft B16F10 model significantly.

4 Discussion

Notably, the inadequate amount of oxygen generation and short-term effects of photosensitizers induced by drug metabolism and clearance in the tumor environment cannot ameliorate the aggravated stuff supply mediated by PDT consumption (10–12), failing efficient and repeated PDT. Therefore, an efficient long-term oxygen supply and drug delivery system should be explored for PDT efficacy improvement and tumor inhibition. Herein, a prolonged oxygen-generating phototherapy hydrogel system (Gel-HCeC-CaO_2) was designed to alleviate tumor hypoxia, prolong drug supply, enhance PDT efficacy, and overcome melanoma. As shown in Figure 5, PSs loaded biocompatible CeNPs nanocarrier (HCeC) was synthesized by an HA-mediated self-assembly method under an alkaline environment, followed by incorporation into a thermo-sensitive hydrogel prepared by simple mixing Pluronic® F127 and F68, the FDA-approved polymers (42). Sufficient oxygen generation was obtained by introducing an O_2-evolving agent CaO_2 into the

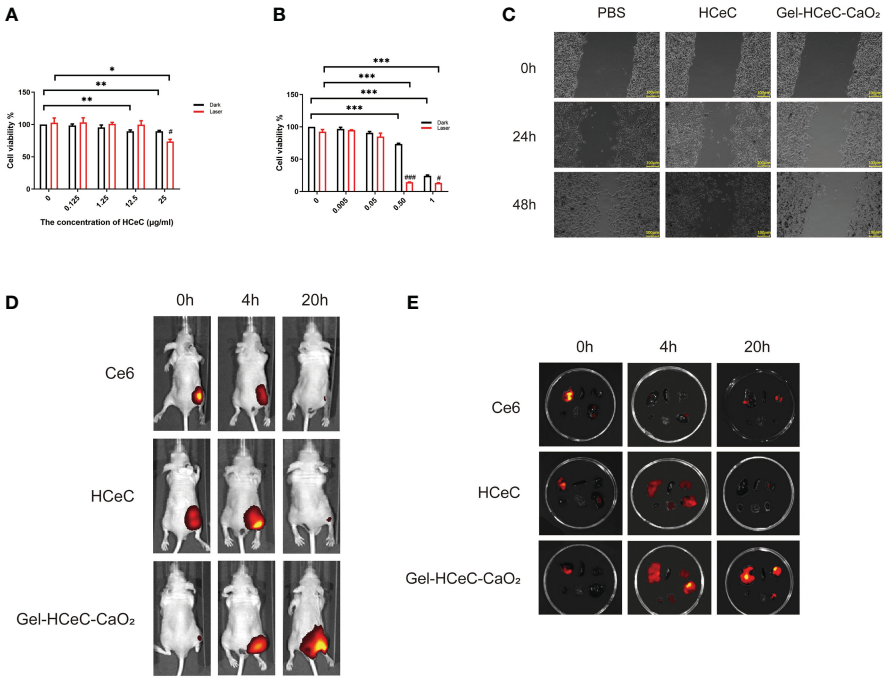

FIGURE 3
In vitro photothermal of HCeC and biodistribution of Gel-HCeC-CaO_2 system. **(A)** The phototoxic effect of HCeC. **(B)** The phototoxic effect of Gel-HCeC-CaO_2 system. **(C)** The migration of B16F10 cells treated with Gel-HCeC-CaO_2 (Laser). **(D)** The biodistribution of Gel-HCeC-CaO_2 *in vivo*. **(E)** Fluorescence imaging of some organs (Top: liver, spleen, kidney; Bottom: heart, lung, tumor). ∗p < 0.05; ∗∗p < 0.01; ∗∗∗p < 0.001.

10.3389/fonc.2023.1126094

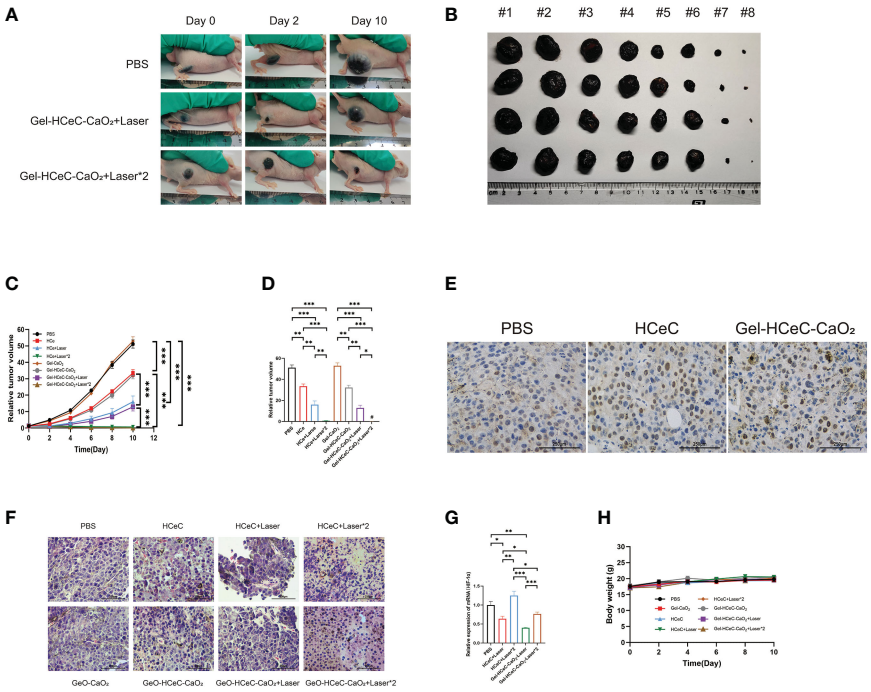

FIGURE 4
In vivo photothermal effect of Gel-HCeC-CaO_2 system. **(A, B)** The tumors of mice in each group were photographed (#1: PBS; #2: Gel-CaO_2; #3: HCeC; #4: Gel-HCeC-CaO_2; #5: HCeC+Laser; #6: Gel-HCeC-CaO_2+Laser; #7: HCeC+Laser*2; #8: Gel-HCeC-CaO_2+Laser*2). **(C, D)** The HCeC and Gel-HCeC-CaO_2 showed significant tumor regression with a reduction of the tumor volume. **(E)** Tunnel assay of the tumor. **(F)** HE staining of tumor. **(G)** The expression of HIF-1 α. **(H)** The body weight of mice. *p < 0.05; **p < 0.01; ***p < 0.001.

hydrogel system, which could react with H_2O to form H_2O_2 and followed produce O_2 catalyzed by catalase-like CeNPs. The prolonged oxygen supply was achieved by the prepared hydrogel. The prepared hydrogel could limit the infiltration of H_2O into the system and moderate the hydrolysis rate of CaO_2, resulting in sustained hypoxia alleviation in tumor tissues. Besides, the prepared hydrogel could act as a sustained delivery system and be easily injected around the tumor, resulting in prolonged drug accumulation. The accumulated

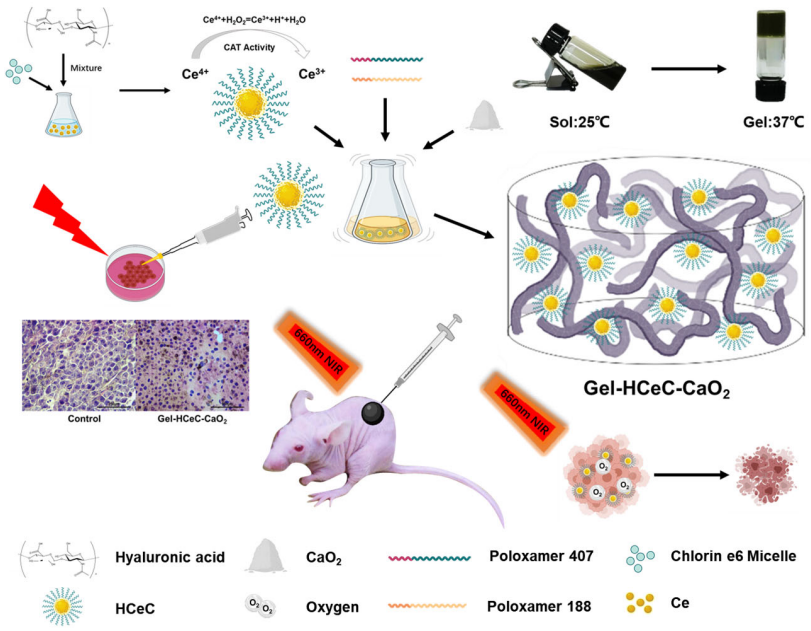

FIGURE 5
Synthesis of the Gel-HCeC-CaO_2 system. The Gel-HCeC-CaO_2 system could alleviate tumor hypoxia microenvironment, prolong drug supply, enhance PDT efficacy, and overcome melanoma.

HCeC entered into tumor cells by endocytosis mediated by CD44, a targeted receptor of HA overexpressed on most of the malignant tumors, resulting in a promoted PSs cellular uptake. Synthetically, a "once injection, repeat irradiation" strategy was achieved through the developed hydrogel system to enhance the PDT efficiency and overcome melanoma.

5 Conclusion

In this study, we prepared a Gel-HCeC-CaO_2 system which showed a significant phototoxic effect of B16F10 tumor by NIR irradiation. The Gel-HCeC-CaO_2 system showed the following advantages: (i) utilized the catalase activity of HCeC to produce O_2; (ii) good retention of the HCeC in the tumor; (iii) no severe systemic toxicity; (iv) alleviate tumor hypoxia environment, meeting the repeated photodynamic therapy strategy and effectively inhibiting tumor metastasis. Therefore, we believe the Gel-HCeC-CaO_2 system will provide a new strategy for the treatment of melanoma, which greatly alleviates the tumor hypoxia microenvironment to improve PDT efficiency.

Data availability statement

The original contributions presented in the study are included in the article/Supplementary Material. Further inquiries can be directed to the corresponding author.

Ethics statement

The animal study was reviewed and approved by Centre for Diseases Prevention and Control of Eastern Theater.

Author contributions

LZ and XL had contributed equally to this work. All authors approved the final manuscript. HL, LZ, and XL designed the study and instructed all experiments. LZ and XL carried out the data analysis and drafted the manuscript. SR, YC, and ZC assisted in performing the experiments. YM, YQ, and HL provided many suggestions on the articles and obtained funding. All authors contributed to the article and approved the submitted version.

Funding

This work was supported by research grants from the National Natural Science Foundation of China (81803173 and 81901555), Natural Science Foundation of Jiangsu Province (SBK2018040981), Incubation Project of Military Medical Science and Technology (20QNPY121), and Youth Science and Technology Project (grant no. (2022)-151).

Conflict of interest

The authors declare that the research was conducted in the absence of any commercial or financial relationships that could be construed as a potential conflict of interest.

Publisher's note

All claims expressed in this article are solely those of the authors and do not necessarily represent those of their affiliated organizations, or those of the publisher, the editors and the reviewers. Any product that may be evaluated in this article, or claim that may be made by its manufacturer, is not guaranteed or endorsed by the publisher.

Supplementary material

The Supplementary Material for this article can be found online at: https://www.frontiersin.org/articles/10.3389/fonc.2023.1126094/full#supplementary-material

References

1. Chen W, Qin M, Chen X, Wang Q, Zhang Z, Sun X. Combining photothermal therapy and immunotherapy against melanoma by polydopamine-coated AlO nanoparticles. *Theranostics* (2018) 8(8):2229–41. doi: 10.7150/thno.24073

2. Marzagalli M, Ebelt ND, Manuel ER. Unraveling the crosstalk between melanoma and immune cells in the tumor microenvironment. *Semin Cancer Biol* (2019) 59:236–50. doi: 10.1016/j.semcancer.2019.08.002

3. Wada-Ohno M, Ito T, Furue M. Adjuvant therapy for Melanoma. *Curr Treat Options Oncol* (2019) 20(8):63. doi: 10.1007/s11864-019-0666-x

4. Gao Y, Wu X, Zhou L, Su Y, Dong C-M. A sweet polydopamine nanoplatform for synergistic combination of targeted chemo-photothermal therapy. *Macromol Rapid Commun* (2015) 36(10):916–22. doi: 10.1002/marc.201500090

5. Spring BQ, Rizvi I, Xu N, Hasan T. The role of photodynamic therapy in overcoming cancer drug resistance. *Photochem Photobiol Sci* (2015) 14(8):1476–91. doi: 10.1039/c4pp00495g

6. Chen Y-C, Liu Y-J, Lee C-L, Pham K-Y, Manoharan D, Thangudu S, et al. Engineering h O and O self-supplying nanoreactor to conduct synergistic chemiexcited photodynamic and calcium-overloaded therapy in orthotopic hepatic Tumors. *Adv Healthc Mater* (2022) 11(20):e2201613. doi: 10.1002/adhm.202201613

7. Kwiatkowski S, Knap B, Przystupski D, Saczko J, Kedzierska E, Knap-Czop K, et al. Photodynamic therapy - mechanisms, photosensitizers and combinations. *Biomedicine Pharmacotherapy = Biomedecine Pharmacotherapie* (2018) 106:1098–107. doi: 10.1016/j.biopha.2018.07.049

8. Tan H-Y, Wang N, Li S, Hong M, Wang X, Feng Y. The reactive oxygen species in macrophage polarization: Reflecting its dual role in progression and treatment of human Diseases. *Oxid Med Cell Longev* (2016) 2016:2795090. doi: 10.1155/2016/2795090

9. Yu W, He X, Yang Z, Yang X, Xiao W, Liu R, et al. Sequentially responsive biomimetic nanoparticles with optimal size in combination with checkpoint blockade for cascade synergetic treatment of breast cancer and lung metastasis. *Biomaterials* (2019) 217:119309. doi: 10.1016/j.biomaterials.2019.119309

10. Fan W, Huang P, Chen X. Overcoming the achilles' heel of photodynamic therapy. *Chem Soc Rev* (2016) 45(23):6488–519. doi: 10.1039/c6cs00616g

11. Li X, Kwon N, Guo T, Liu Z, Yoon J. Innovative strategies for hypoxic-tumor photodynamic Therapy. *Angewandte Chemie (International Ed In English)* (2018) 57 (36):11522–31. doi: 10.1002/anie.201805138

12. Zhao C, Tong Y, Li X, Shao L, Chen L, Lu J, et al. Photosensitive nanoparticles combining vascular-independent intratumor distribution and on-demand oxygen-depot delivery for enhanced cancer photodynamic Therapy. *Small* (2018) 14(12):e1703045. doi: 10.1002/smll.201703045

13. Zheng D-W, Li B, Li C-X, Fan J-X, Lei Q, Li C, et al. Carbon-Dot-Decorated carbon nitride nanoparticles for enhanced photodynamic therapy against hypoxic tumor *via* water Splitting. *ACS Nano* (2016) 10(9):8715–22. doi: 10.1021/acsnano.6b04156

14. Miyoshi A, Nishioka S, Maeda K. Water splitting on rutile TiO -based Photocatalysts. *Chemistry* (2018) 24(69):18204–19. doi: 10.1002/chem.201800799

15. Yang Z, Wang J, Liu S, Li X, Miao L, Yang B, et al. Defeating relapsed and refractory malignancies through a nano-enabled mitochondria-mediated respiratory inhibition and damage pathway. *Biomaterials* (2020) 229:119580. doi: 10.1016/j.biomaterials.2019.119580

16. Zhang N, Tan Y, Yan L, Zhang C, Xu M, Guo H, et al. Modulation of tumor hypoxia by pH-responsive liposomes to inhibit mitochondrial respiration for enhancing sonodynamic Therapy. *Int J Nanomedicine* (2020) 15:5687–700. doi: 10.2147/IJN.S256038

17. Wang T, Zhang H, Han Y, Liu H, Ren F, Zeng J, et al. Light-enhanced O-evolving nanoparticles boost photodynamic therapy to elicit antitumor Immunity. *ACS Appl Mater Interfaces* (2019) 11(18):16367–79. doi: 10.1021/acsami.9b03541

18. Zhang Y, Shen T-T, Kirillov AM, Liu W-S, Tang Y. NIR light/H2O2-triggered nanocomposites for a highly efficient and selective synergistic photodynamic and photothermal therapy against hypoxic tumor cells. *Chem Commun (Camb)* (2016) 52 (51):7939–42. doi: 10.1039/C6CC02571D

19. Hei Y, Teng B, Zeng Z, Zhang S, Li Q, Pan J, et al. Multifunctional immunoliposomes combining catalase and PD-L1 antibodies overcome tumor hypoxia and enhance immunotherapeutic effects against Melanoma. *Int J Nanomedicine* (2020) 15:1677–91. doi: 10.2147/IJN.S225807

20. Shi C, Li M, Zhang Z, Yao Q, Shao K, Xu F, et al. Catalase-based liposomal for reversing immunosuppressive tumor microenvironment and enhanced cancer chemo-photodynamic therapy. *Biomaterials* (2020) 233:119755. doi: 10.1016/j.biomaterials.2020.119755

21. Gao D, Gao Y, Shen J, Wang Q. Modified nanoscale metal organic framework-based nanoplatforms in photodynamic therapy and further applications. *Photodiagnosis Photodyn Ther* (2020) 32:102026. doi: 10.1016/j.pdpdt.2020.102026

22. Lan G, Ni K, Veroneau SS, Feng X, Nash GT, Luo T, et al. Titanium-based nanoscale metal-organic framework for type I photodynamic Therapy. *J Am Chem Soc* (2019) 141(10):4204–8. doi: 10.1021/jacs.8b13804

23. Cheng X, He L, Xu J, Fang Q, Yang L, Xue Y, et al. Oxygen-producing catalase-based prodrug nanoparticles overcoming resistance in hypoxia-mediated chemo-photodynamic therapy. *Acta Biomater* (2020) 112:234–49. doi: 10.1016/j.actbio.2020.05.035

24. Zhang R, Song X, Liang C, Yi X, Song G, Chao Y, et al. Catalase-loaded cisplatin-prodrug-constructed liposomes to overcome tumor hypoxia for enhanced chemo-radiotherapy of cancer. *Biomaterials* (2017) 138:13–21. doi: 10.1016/j.biomaterials.2017.05.025

25. Wu J, Wang X, Wang Q, Lou Z, Li S, Zhu Y, et al. Nanomaterials with enzyme-like characteristics (nanozymes): Next-generation artificial enzymes (II). *Chem Soc Rev* (2019) 48(4):1004–76. doi: 10.1039/C8CS00457A

26. Song W, Zhao B, Wang C, Ozaki Y, Lu X. Functional nanomaterials with unique enzyme-like characteristics for sensing applications. *J Mater Chem B* (2019) 7(6):850–75. doi: 10.1039/C8TB02878H

27. Gao L, Zhuang J, Nie L, Zhang J, Zhang Y, Gu N, et al. Intrinsic peroxidase-like activity of ferromagnetic nanoparticles. *Nat Nanotechnol* (2007) 2(9):577–83. doi: 10.1038/nnano.2007.260

28. Song D, Li T, Wei Y-Y, Xu Z-R. Controlled formation of porous CuCoO nanorods with enhanced oxidase and catalase catalytic activities using bimetal-organic frameworks as temp lates. *Colloids Surf B Biointerfaces* (2020) 188:110764. doi: 10.1016/j.colsurfb.2019.110764

29. Liu R, Zuo L, Huang X, Liu S, Yang G, Li S, et al. Colorimetric determination of lead(II) or mercury(II) based on target induced switching of the enzyme-like activity of metallothionein-stabilized copper nanoclusters. *Mikrochim Acta* (2019) 186(4):250. doi: 10.1007/s00604-019-3360-6

30. Zhang T, Lu Y, Luo G. Synthesis of hierarchical iron hydrogen phosphate crystal as a robust peroxidase mimic for stable H_2O_2 detection. *ACS Appl Mater Interfaces* (2014) 6 (16):14433–8. doi: 10.1021/am503708a

31. Guo J, Wang Y, Zhao M. 3D flower-like ferrous(II) phosphate nanostructures as peroxidase mimetics for sensitive colorimetric detection of hydrogen peroxide and glucose at nanomolar level. *Talanta* (2018) 182:230–40. doi: 10.1016/j.talanta.2018.01.080

32. Sun Z, Zhang N, Si Y, Li S, Wen J, Zhu X, et al. High-throughput colorimetric assays for mercury(II) in blood and wastewater based on the mercury-stimulated catalytic activity of small silver nanoparticles in a temperature-switchable gelatin matrix. *Chem Commun (Camb)* (2014) 50(65):9196–9. doi: 10.1039/C4CC03851G

33. Chen L, Sha L, Qiu Y, Wang G, Jiang H, Zhang X, et al. An amplified electrochemical aptasensor based on hybridization chain reactions and catalysis of silver nanoclusters. *Nanoscale* (2015) 7(7):3300–8. doi: 10.1039/C4NR06664B

34. Karim MN, Anderson SR, Singh S, Ramanathan R, Bansal V. Nanostructured silver fabric as a free-standing NanoZyme for colorimetric detection of glucose in urine. *Biosens Bioelectron* (2018) 110:8–15. doi: 10.1016/j.bios.2018.03.025

35. Singh R, Belgamwar R, Dhiman M, Polshettiwar V. Dendritic fibrous nano-silica supported gold nanoparticles as an artificial enzyme. *J Mater Chem B* (2018) 6(11):1600–4. doi: 10.1039/C8TB00310F

36. Drozd M, Pietrzak M, Parzuchowski PG, Malinowska E. Pitfalls and capabilities of various hydrogen donors in evaluation of peroxidase-like activity of gold nanoparticles. *Anal Bioanal Chem* (2016) 408(29):8505–13. doi: 10.1007/s00216-016-9976-z

37. Charbgoo F, Ahmad MB, Darroudi M. Cerium oxide nanoparticles: Green synthesis and biological applications. *Int J Nanomedicine* (2017) 12:1401–13. doi: 10.2147/IJN.S124855

38. Sadidi H, Hooshmand S, Ahmadabadi A, Javad Hosseini S, Baino F, Vatanpour M, et al. Cerium oxide nanoparticles (Nanoceria): Hopes in soft tissue Engineering. *Molecules (Basel Switzerland)* (2020) 25(19):4559. doi: 10.3390/molecules25194559

39. Celardo I, Pedersen JZ, Traversa E, Ghibelli L. Pharmacological potential of cerium oxide nanoparticles. *Nanoscale* (2011) 3(4):1411–20. doi: 10.1039/c0nr00875c

40. Lin W, Huang Y-W, Zhou X-D, Ma Y. Toxicity of cerium oxide nanoparticles in human lung cancer cells. *Int J Toxicol* (2006) 25(6):451–7. doi: 10.1080/10915810600959543

41. Alili L, Sack M, Karakoti AS, Teuber S, Puschmann K, Hirst SM, et al. Combined cytotoxic and anti-invasive properties of redox-active nanoparticles in tumor-stroma interactions. *Biomaterials* (2011) 32(11):2918–29. doi: 10.1016/j.biomaterials.2010.12.056

42. Lin Z, Gao W, Hu H, Ma K, He B, Dai W, et al. Novel thermo-sensitive hydrogel system with paclitaxel nanocrystals: High drug-loading, sustained drug release and extended local retention guaranteeing better efficacy and lower toxicity. *J Controlled Release Off J Controlled Release Soc* (2014) 174:161–70. doi: 10.1016/j.jconrel.2013.10.026

43. Liu Y, Lu W-L, Wang J-C, Zhang X, Zhang H, Wang X-Q, et al. Controlled delivery of recombinant hirudin based on thermo-sensitive pluronic F127 hydrogel for subcutaneous administration: *In vitro* and *in vivo* characterization. *J Controlled Release Off J Controlled Release Soc* (2007) 117(3):387–95. doi: 10.1016/j.jconrel.2006.11.024

44. Zhang N, Xu X, Zhang X, Qu D, Xue L, Mo R, et al. Nanocomposite hydrogel incorporating gold nanorods and paclitaxel-loaded chitosan micelles for combination photothermal-chemotherapy. *Int J Pharm* (2016) 497(1-2):210–21. doi: 10.1016/j.ijpharm.2015.11.032

45. Li H, Liu C, Zeng Y-P, Hao Y-H, Huang J-W, Yang Z-Y, et al. Nanoceria-mediated drug delivery for targeted photodynamic therapy on drug-resistant breast Cancer. *ACS Appl Mater Interfaces* (2016) 8(46):31510–23. doi: 10.1021/acsami.6b07338

46. Liang X, Ye X, Wang C, Xing C, Miao Q, Xie Z, et al. Photothermal cancer immunotherapy by erythrocyte membrane-coated black phosphorus formulation. *J Controlled Release Off J Controlled Release Soc* (2019) 296:150–61. doi: 10.1016/j.jconrel.2019.01.027

47. Ullah I, Karthik G-M, Alkodsi A, Kjällquist U, Stålhammar G, Lövrot J, et al. Evolutionary history of metastatic breast cancer reveals minimal seeding from axillary lymph nodes. *J Clin Invest* (2018) 128(4):1355–70. doi: 10.1172/JCI96149

48. Zhang L, Tian G, Huang L, Zhou M, Zhu J, Yi L, et al. Pterostilbene attenuates intestinal epithelial barrier loss induced by high loading intensity of exercise. *Front Nutr* (2022) 9:965180. doi: 10.3389/fnut.2022.965180

49. Colon J, Herrera L, Smith J, Patil S, Komanski C, Kupelian P, et al. Protection from radiation-induced pneumonitis using cerium oxide nanoparticles. *Nanomedicine Nanotechnology Biology Med* (2009) 5(2):225–31. doi: 10.1016/j.nano.2008.10.003

50. Salwowska NM, Bebenek KA, Żądło DA, Wcisło-Dziadecka DL. Physiochemical properties and application of hyaluronic acid: A systematic review. *J Cosmet Dermatol* (2016) 15(4):520–6. doi: 10.1111/jocd.12237

51. Yang Z, Li Y, Sun F, Hou H, Xing L, Wang Z, et al. Improved stability and enhanced anti-tumor activity of hyaluronic acid modified ES2-AF nanoparticle-like Conjugate. *J BioMed Nanotechnol* (2019) 15(8):1781–91. doi: 10.1166/jbn.2019.2808

52. Abatangelo G, Vindigni V, Avruscio G, Pandis L, Brun P. Hyaluronic acid: Redefining its role. *Cells* (2020) 9(7):1743. doi: 10.3390/cells9071743

53. Kopeček J. Hydrogels from soft contact lenses and implants to self-assembled nanomaterials. *J Polymer Sci Part A Polymer Chem* (2009) 47(22):5929–46. doi: 10.1002/pola.23607

54. Wang Q, Chen J, Zhang H, Wu W, Zhang Z, Dong S, et al. Porous CoO nanoplates with pH-switchable peroxidase- and catalase-like activity. *Nanoscale* (2018) 10 (40):19140–6. doi: 10.1039/C8NR06162A

55. Bao L, Chen Y, Lai H-T, Wu S-Y, Wang JE, Hatanpaa KJ, et al. Methylation of hypoxia-inducible factor (HIF)-1α by G9a/GLP inhibits HIF-1 transcriptional activity and cell migration. *Nucleic Acids Res* (2018) 46(13):6576–91. doi: 10.1093/nar/gky449